

Intensity-and-Landmark-Driven, Inverse Consistent, B-Spline Registration and Analysis for Lung Imagery

Kunlin Cao^{1,3}, Gary E. Christensen^{1,3}, Kai Ding^{2,3}, and
Joseph M. Reinhardt^{2,3,*}

¹ Department of Electrical and Computer Engineering

² Department of Biomedical Engineering

³ The Iowa Institute for Biomedical Imaging and

The Iowa Comprehensive Lung Imaging Center

The University of Iowa, Iowa City, 52242

Abstract. Lung disease is the number three cause of death in America. Measuring local volume deformation from lung image registration may provide a non-invasive approach for detecting and classifying diseases and provide a means for measuring how these diseases respond to intervention. 3D lung CT images contain easily identifiable landmarks such as airway-tree and vascular-tree branch points that can be used for registration and validation. Intensity-based registration methods complement landmark registration methods by providing dense correspondence information since landmarks only provide sparse correspondence information. Intensity-based registration performs best in regions of strong contrast such as between the lung parenchyma and the chest wall, and between the parenchyma and the blood vessels and larger airways. This paper describes a Landmark, Inverse consistent, Tissue volume preserving, B-Spline (LITS) registration algorithm which can be used to measure local lung volume deformation. This method extends the original tissue volume preserving method by adding landmark information and inverse consistency constraint. LITS registration was applied on three subjects to match lung datasets acquired at functional residual capacity and total lung capacity. The registration errors are small compared to the large overall deformations. Sensitivity analysis was performed by changing node spacing of the parameterization and shows that finer B-Spline lattice setting can reveal more details of the feature deformation.

1 Introduction

The role of the respiratory system is to provide gas exchange. Lung tissue ventilation depends on the complex interrelationships between the lungs, rib cage, diaphragm, and abdomen. Many lung diseases, such as lung cancer and chronic obstructive pulmonary disease, alter the material properties of the lung tissue,

* Joseph M. Reinhardt is a shareholder in VIDA Diagnostics, Inc.

thus altering local and global region ventilation. Therefore, it is important to measure regional lung volume change for disease detection and tracking, and to help provide a better understanding of the normal and abnormal lung.

Imaging allows non-invasive study of lung behavior and image registration can be used to examine the lung deformation. Local lung expansion can be estimated using registration to match images acquired at different levels of inflation. Tissue expansion (and thus, specific volume change) can be estimated by calculating the Jacobian of the transformation [1]. It is important to ensure the accuracy of registration result since the Jacobian is computed from the transformation.

Guerrero et al. used two CT images acquired at different lung inflation levels and optical flow image registration to estimate regional ventilation to identify functioning vs. non-functioning lung tissue for radiotherapy treatment planning [2, 3]. Christensen et al. used consistent image registration to match images across cine-CT sequences to estimate local tissue expansion and contraction over the breathing cycle [4]. These methods assume that corresponding points in both images have the same grayscale intensities. However, this is not true for the lung because the tissue density changes as the lung inflates and deflates. CT intensity is a measure of tissue density and therefore changes as the tissue density changes. Efforts have been made to take this intensity change into consideration. Sarrut et al. [5] added a preprocessing step to artificially correct the intensity range. Gorbunova et al. [6] modified the sum of squared difference measure by adding total lung weight and regional volume change information to preserve lung weight globally and locally. Yin et al. [7] used a new similarity cost by preserving lung tissue volume. All these methods have demonstrated improved registration accuracy.

Most registration methods mentioned above use volumetric based similarity functions to compute a cost for mismatched subvolumes but give no cost to mismatched landmarks, contours, or surfaces. Mismatched landmarks, contours, and surfaces have zero measure under the volume integral and thus are difficult to match using a volumetric similarity function. Landmark based image registration has the advantage of matching landmarks either exactly or inexactly based on the confidence of the landmark location. A major limitation of landmark-based approaches is that they interpolate the transformation between the landmarks and ignore intensity information.

Combining landmark and intensity information together helps reduce the limitations of each method. This paper describes a Landmark, Inverse consistent, Tissue volume preserving, B-Spline (LITS) registration algorithm for matching lung CT images with large pressure changes. The sensitivity of this registration method to feature size is analyzed by changing the spatial resolution of the transformation parameterization.

2 Methods

2.1 Data Acquisition

Pairs of volumetric CT data sets from three normal human subjects scanned at supine orientation were used in the study. For subject 1, data was acquired at functional residual capacity (FRC) with 26.3% of the vital capacity (VC) and total lung capacity (TLC) with 95.7% of the VC. For subject 2, data was acquired at FRC with 21.8% of the VC and TLC with 95.6% of the VC. For subject 3, data was acquired at FRC with 11.0% of the VC and TLC with 68.9% of the VC. Volumetric data sets were acquired at a section spacing of 0.5 mm and a reconstruction matrix of 512×512 . In-plane pixel spatial resolution is $0.6 \text{ mm} \times 0.6 \text{ mm}$. The data were resized to spatial resolution $1 \text{ mm} \times 1 \text{ mm} \times 1 \text{ mm}$ to use less memory and reduce the time for registration.

The parenchyma regions in the FRC and TLC data sets were segmented using Hu et al [8]. An automatic lobe segmentation algorithm [9] was used to segment the parenchyma regions into five different lobes. Three fissures were identified where the lobe segmentations touched each other. The landmarks in FRC image were selected as the bifurcations of the vessel tree. A semi-automatic system [10] was used to guide the observer to find the corresponding landmarks in the TLC image. An expert selected 160, 150, and 105 landmark pairs for the three subjects, respectively. Fig. 1 shows the corresponding landmarks (green points) selected at vessel-tree branch points on FRC and TLC scans of one subject.

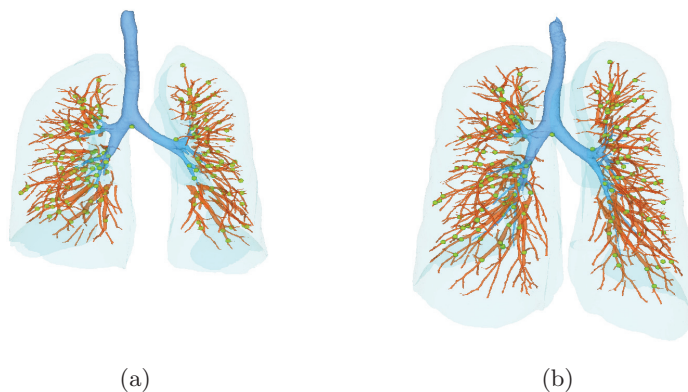


Fig. 1. Landmarks selected at vessel-tree branch points on (a) FRC, and (b) TLC scans of one subject.

2.2 Inverse Consistent Image Registration

Let I_1 and I_2 denote two 3D images on the domain $\Omega = [0, 1]^3$ and let $\mathbf{x} = (x_1, x_2, x_3)^T \in \Omega$ define a voxel coordinate in the domain Ω . The goal of a registration procedure is to find an optimal transformation (correspondence map) \mathbf{h} that matches the corresponding coordinates of the two images. The transformation \mathbf{h} is defined as a (3×1) vector-valued function defined on Ω . The vector-valued function $\mathbf{u} = \mathbf{h}(\mathbf{x}) - \mathbf{x}$ is called the displacement field since it represents the transformation in terms of a displacement from a location \mathbf{x} .

The forward transformation \mathbf{h}_{12} deforms I_1 to I_2 and the reverse transformation \mathbf{h}_{21} deform I_2 to I_1 . For intra-subject registration, a meaningful transformation should be one-to-one mapping, i.e., each point in image I_1 is mapped to only one point in image I_2 and vice versa. However, many unidirectional image registration techniques have the problem that their similarity cost function does not uniquely determine the correspondence between two images. The reason is that the local minima of similarity cost functions cause the estimated forward mapping \mathbf{h}_{12} to be different from the inverse of the estimated reverse mapping \mathbf{h}_{21}^{-1} . To overcome correspondence ambiguities, the transformations \mathbf{h}_{12} and \mathbf{h}_{21} are jointly estimated in the LITS registration algorithm. Ideally, \mathbf{h}_{12} and \mathbf{h}_{21} should be inverses of one another, i.e., $\mathbf{h}_{12} = \mathbf{h}_{21}^{-1}$.

Depending on the application, different criteria for image matching are designed to find the best correspondence mapping between two images. When registering intra-subject CT images of the lung, many landmarks such as branch points of the airway and vascular trees can be easily identified and utilized for image registration and validation. The LITS registration algorithm is driven both by intensity and by minimizing the Euclidean distance between corresponding landmarks. The landmark error for a landmark on one image measures the distance from its estimated position to real position on the second image. A symmetric landmark similarity cost is defined to minimize the landmark errors,

$$C_{\text{LMK}} = \sum_k \|\mathbf{p}_k - \mathbf{h}_{12}(\mathbf{q}_k)\|^2 + \|\mathbf{q}_k - \mathbf{h}_{21}(\mathbf{p}_k)\|^2, \quad (1)$$

where \mathbf{p}_k and \mathbf{q}_k are the location of landmark k on image I_1 and I_2 , respectively.

The intensity matching criterion is used to register similar grayscale patterns in two images. To take the variation of intensity during respiration into account, the sum of squared tissue volume difference (SSTVD) [7] is used as the intensity similarity criterion to preserve tissue volume. This similarity criterion aims to minimize the local difference of tissue volume inside the lungs scanned at different pressure levels. Assume the Hounsfield units (HU) of CT lung images are primarily contributed by tissue and air. Then the tissue volume in a voxel at position \mathbf{x} can be estimated as $V(\mathbf{x}) = v(\mathbf{x}) \frac{HU(\mathbf{x}) - HU_{\text{air}}}{HU_{\text{tissue}} - HU_{\text{air}}}$ where $v(\mathbf{x})$ is the volume of voxel \mathbf{x} . It is assumed that $HU_{\text{air}} = -1000$ and $HU_{\text{tissue}} = 55$. At location \mathbf{x} , let $I_1(\mathbf{x})$ and $I_2(\mathbf{x})$ be the intensity values (HU), $v_1(\mathbf{x})$ and $v_2(\mathbf{x})$ be the voxel volumes, and $V_1(\mathbf{x})$ and $V_2(\mathbf{x})$ be the tissue volumes in the voxel of

images I_1 and I_2 , respectively. The intensity similarity cost is defined as

$$\begin{aligned} C_{\text{SSTVD}} &= \int_{\Omega} \left\{ [V_2(\mathbf{x}) - V_1(\mathbf{h}_{12}(\mathbf{x}))]^2 + [V_1(\mathbf{x}) - V_2(\mathbf{h}_{21}(\mathbf{x}))]^2 \right\} d\mathbf{x} \\ &= \int_{\Omega} \left\{ \left[v_2(\mathbf{x}) \frac{I_2(\mathbf{x}) + 1000}{1055} - v_1(\mathbf{h}_{12}(\mathbf{x})) \frac{I_1(\mathbf{h}_{12}(\mathbf{x})) + 1000}{1055} \right]^2 \right. \\ &\quad \left. + \left[v_1(\mathbf{x}) \frac{I_1(\mathbf{x}) + 1000}{1055} - v_2(\mathbf{h}_{21}(\mathbf{x})) \frac{I_2(\mathbf{h}_{21}(\mathbf{x})) + 1000}{1055} \right]^2 \right\} d\mathbf{x}. \quad (2) \end{aligned}$$

The Jacobian of a transformation estimates the pointwise volume change produced by mapping an image through the transformation. Thus, the tissue volume in image I_1 and I_2 are related by $v_1(\mathbf{h}_{12}(\mathbf{x})) = v_2(\mathbf{x}) \cdot J(\mathbf{h}_{12}(\mathbf{x}))$ and $v_2(\mathbf{h}_{21}(\mathbf{x})) = v_1(\mathbf{x}) \cdot J(\mathbf{h}_{21}(\mathbf{x}))$ where $J(\mathbf{h}_{12}(\mathbf{x}))$ and $J(\mathbf{h}_{21}(\mathbf{x}))$ are the Jacobian values of the forward and reverse transformations at position \mathbf{x} , respectively. In this way, the intensity similarity cost can be rewritten as

$$\begin{aligned} C_{\text{SSTVD}} &= \int_{\Omega} \left\{ \left[v_2(\mathbf{x}) \frac{I_2(\mathbf{x}) + 1000}{1055} - v_2(\mathbf{x}) J(\mathbf{h}_{12}(\mathbf{x})) \frac{I_1(\mathbf{h}_{12}(\mathbf{x})) + 1000}{1055} \right]^2 \right. \\ &\quad \left. + \left[v_1(\mathbf{x}) \frac{I_1(\mathbf{x}) + 1000}{1055} - v_1(\mathbf{x}) J(\mathbf{h}_{21}(\mathbf{x})) \frac{I_2(\mathbf{h}_{21}(\mathbf{x})) + 1000}{1055} \right]^2 \right\} d\mathbf{x}. \quad (3) \end{aligned}$$

Minimizing the symmetric cost functions given in Equations 1 and 3 does not guarantee that \mathbf{h}_{12} and \mathbf{h}_{21} are inverses of each other. In order to couple the estimation of \mathbf{h}_{12} and \mathbf{h}_{21} , an inverse consistency constraint [11] is imposed which is minimized when $\mathbf{h}_{12} = \mathbf{h}_{21}^{-1}$:

$$C_{\text{ICC}} = \int_{\Omega} \|\mathbf{h}_{12}(\mathbf{x}) - \mathbf{h}_{21}^{-1}(\mathbf{x})\|^2 d\mathbf{x} + \int_{\Omega} \|\mathbf{h}_{21}(\mathbf{x}) - \mathbf{h}_{12}^{-1}(\mathbf{x})\|^2 d\mathbf{x}. \quad (4)$$

The transformation is said to be inverse-consistent when $\mathbf{h}_{12} = \mathbf{h}_{21}^{-1}$.

2.3 Transformation Parameterization and Estimation

The B-Splines based parameterization was used to represent the forward and reverse transformations to make it easy to combine landmark with an intensity based registration approach as shown by Kybic and Unser [12, 13]. Let $\phi_i = [\phi_x(\mathbf{x}_i), \phi_y(\mathbf{x}_i), \phi_z(\mathbf{x}_i)]^T$ be the i -th control point values on lattice G along each direction. The transformation is defined as

$$\mathbf{h}(\mathbf{x}) = \mathbf{x} + \sum_{i \in G} \phi_i \beta^{(3)}(\mathbf{x} - \mathbf{x}_i), \quad (5)$$

where $\mathbf{x}_i = (x_i, y_i, z_i)^T$ is the coordinate vector of a lattice point, $\beta^{(3)}(\mathbf{x}) = \beta^{(3)}(x)\beta^{(3)}(y)\beta^{(3)}(z)$ is a separable convolution kernel, and $\beta^{(3)}(x)$ is the uniform cubic B-Spline basis function.

The total cost $C_{total} = \alpha C_{LMK} + \rho C_{SSTVD} + \chi C_{ICC}$ is optimized using a limited-memory, quasi-Newton minimization method with bounds (L-BFGS-B) [14] algorithm, which is well suited for optimization with high dimensionality of parameter space. At each iteration, it was assumed that the functions $\mathbf{h}_{12}^{-1}(\mathbf{x})$ and $\mathbf{h}_{21}^{-1}(\mathbf{x})$ were constant to reduce computation complexity. α , ρ and χ are weights to adjust the significance of the three cost terms. For the study reported in this paper, the weights $\alpha = 4$, $\rho = 1$ and $\chi = 10^{-5}$ were selected by trial and error to give the best trade-off between intensity similarity and landmark similarity.

2.4 Assessment of Image Registration Accuracy

Point, surface, and volume measures were used to assess the accuracy of the image registration results. For each pair of data, 85% – 90% of landmarks were used for registration, and the remaining (15 landmarks) were used for validation. The landmark error measures the errors of validation landmarks, which are distributed in five lobes and were selected randomly.

The Fissure Positioning Error (FPE) is determined by comparing the distance between the transformed fissure and target fissure. The FPE is defined as the minimum distance between a point on the deformed fissure and the closest point on the corresponding target fissure. Mathematically, this can be stated as $FPE(\mathbf{x}) = \min_{\mathbf{y} \in F_2} d(\mathbf{x}, \mathbf{h}_{12}(\mathbf{y}))$ for a given point \mathbf{x} in F_1 , where F_1 (F_2 , resp.) is the set of all points in the fissure in image I_1 (I_2 , resp.) and $d(\cdot)$ defines the Euclidean distance.

The Relative Overlap (RO) statistic was used to measure how well corresponding regions of the parenchyma agreed with each other. The RO for forward registration is given by $RO(S_1 \circ \mathbf{h}_{12}, S_2) = \frac{(S_1 \circ \mathbf{h}_{12}) \cap S_2}{(S_1 \circ \mathbf{h}_{12}) \cup S_2}$ where S_1 and S_2 are segmentations of parenchyma regions on images I_1 and I_2 , respectively. $RO = 1$ implies a perfect segmentation matching.

3 Experiments and Results

3.1 Registration Accuracy

The LITS registration method described in Section 2 was used to register the parenchyma region of the three subjects. Small Deformation Inverse Consistent Linear Elastic [11] (SICLE) registration, which uses the sum of squared difference as similarity cost and its transformation represented by Fourier coefficients, was used to register the three pairs of data for comparison. The mean and standard deviation of different errors for both forward (FRC to TLC) and reverse (TLC to FRC) transformations are shown in Fig. 2 (a)-(c). For this study, the SICLE algorithm used $3 \times 24 \times 24 \times 24 = 41,472$ parameters and LITS estimated $3 \times 25 \times 25 \times 25 = 46,875$ parameters (16 mm grid spacing) to parameterize each transformation. The average distance of validation landmarks across three subjects was 25.18 mm before registration (15 validation landmarks for each

subject). The SICLE algorithm reduced the landmark error to 7.53 mm and the LITS algorithm reduced it to 1.26 mm. The average fissure positioning error across three subjects was 8.22 mm before registration, 4.05 mm after using SICLE registration and 1.65 mm after using LITS registration. Both SICLE and LITS achieve around 0.96 relative overlap.

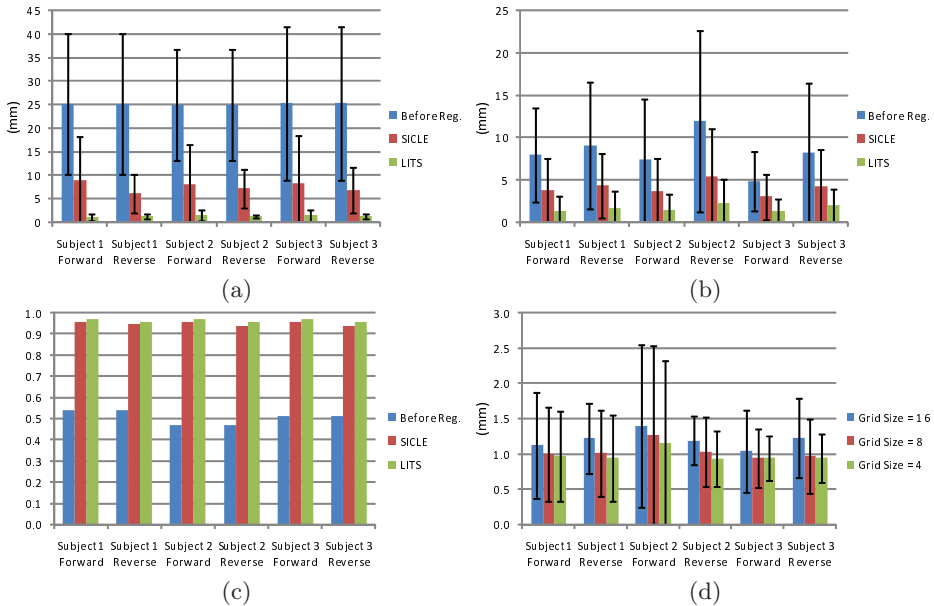


Fig. 2. The registration errors of experiments on three subjects. (a)-(c) show the mean and standard deviation for landmark error, fissure positioning error, and relative overlap using SICLE and LITS, respectively. (d) shows the mean and standard deviation of landmark error using LITS by varying the grid sizes.

3.2 B-Spline Sensitivity Analysis

The grid size of the B-Spline lattice decides the number of parameters estimated in the registration process. Three choices of grid size (4 mm, 8 mm and 16 mm) were tested using LITS to study how the grid size affected the registration results. The fissure positioning error and relative overlap error were nearly the same for different grid size. Fig. 2 (d) shows the landmark accuracy using different grid sizes. Smaller grid sizes have slightly lower errors.

The Jacobian of a transformation can be used to estimate the pointwise volume expansion and contraction of the transformation. Using a Lagrangian reference frame, local tissue expansion corresponds to a Jacobian greater than one and local tissue contraction corresponds to a Jacobian less than one. The Jacobian map shown in Fig. 3 reflects the fact that vessels have little deformation

during the respiratory cycle while lung tissues and airways expand/contract a lot.

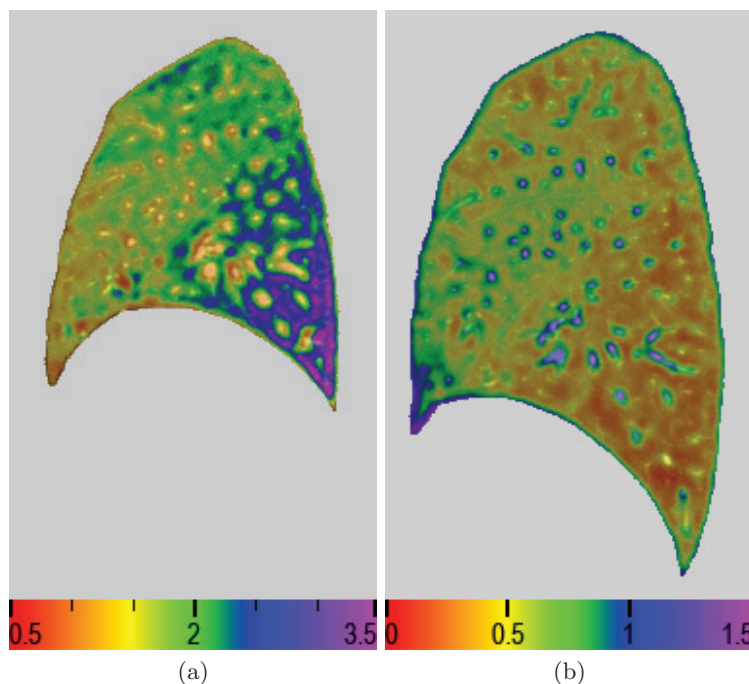


Fig. 3. The Jacobian maps on a sagittal slice. (a) Jacobian on FRC image showing local volume deformation in inhalation stage; and (b) Jacobian on TLC image showing local volume deformation in exhalation stage. The B-Spline lattice grid size is 4 mm for LITS.

The Jacobian difference between vessels and other lung regions can be utilized to reveal how small a structure can be detected as the grid size of the B-Spline lattice is changed. Using LITS with different lattice grid size settings and SICLE, the Jacobian maps on the same sagittal slice of a FRC data are compared in Fig. 4. Fig. 5 shows the effect of changing grid size to detect vessels of different sizes and to detect two vessels in real images based on LITS resulting Jacobians (FRC to TLC). The Jacobian of the transformation produced using SICLE is also plotted for comparison. Each picture in Fig. 5 plots the $1/\text{Jacobian}$ (left vertical axis) and HU value (right vertical axis) changes along a line profile. The horizontal axis lists the point numbers on the line profile.

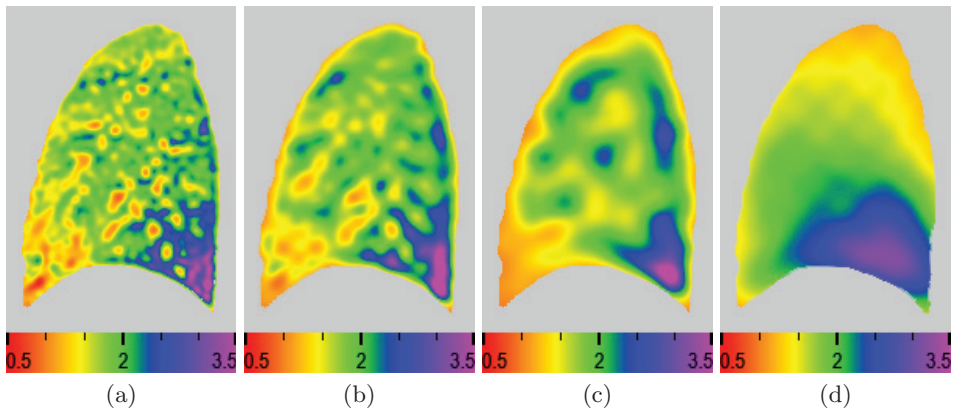


Fig. 4. The Jacobian maps on the same sagittal slice of a FRC data resulting from LITS with the B-Spline lattice grid size of (a) 4 mm, (b) 8 mm, and (c) 16 mm. (d) shows the Jacobian map resulting from SICLE.

4 Discussion

Fig. 2 (a)-(c) shows that both SICLE and LITS match the boundaries of two lung parenchyma well but LITS has much lower landmark error and fissure positioning error compared to SICLE. There are two reasons for this. First, LITS has vessel tree landmark information in the registration while SICLE does not. Secondly, SICLE uses the sum of squared difference as similarity cost which assumes the grayscales for corresponding voxels in two images are the same. However, the assumption is not true in the lung CT images due to the tissue density change as air goes into the lung during inhalation. Taking this into consideration, the SSTVD similarity cost aims to minimize the lung tissue volume change during the respiratory process. This similarity cost performs better on vessels and fissures for intra-subject lung CT image registration.

Changing the grid size of the B-Spline lattice in LITS has little effect on the landmark error, fissure positioning error, and relative overlap measurements. This is because those measures evaluate the accuracy on mostly vessel branch points, fissures and boundaries which have strong intensity contrast with their neighboring region and can be matched through optimizing the intensity and landmark similarity cost. But finer grid setting can give a more detailed deformation map, as shown in Fig. 4 (a)-(c). Fig. 4 (d) shows that the 3D Fourier basis parameterization that used the 24 lowest harmonics in the 3 coordinate directions ($3 \times 24 \times 24 \times 24$ parameters) produced a smoother Jacobian map than the B-Spline basis. This result may suggest that the local support of the B-Spline basis is better for detecting small features compared to the infinite support of the Fourier series basis. Fig. 5 shows that smaller grid sizes are required to detect narrow vessels and to separate nearby vessels. This analysis can help us choose the B-Spline lattice spacing setting to detect the deformation of features with

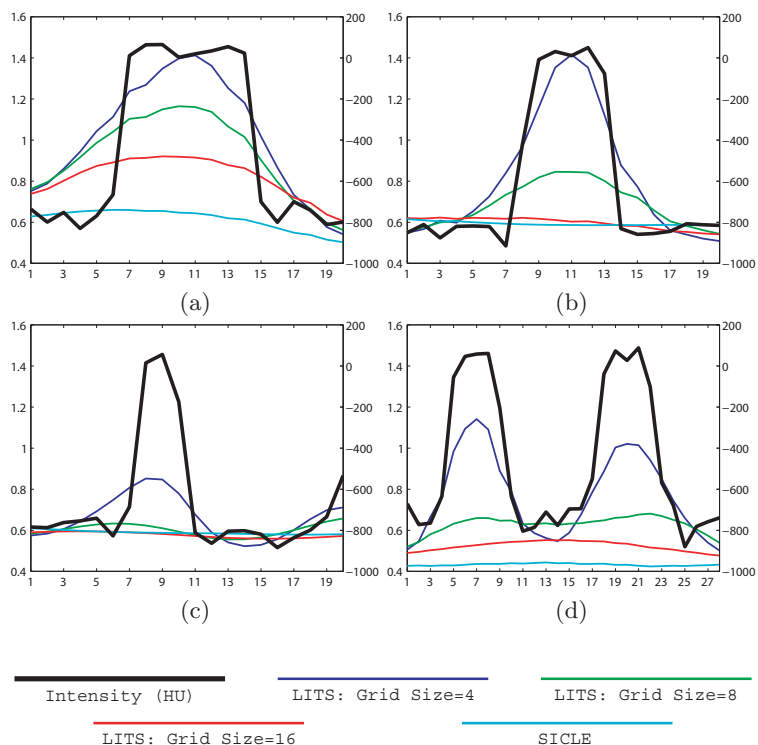


Fig. 5. The changes of $1/\text{Jacobian}$ (left vertical axis) and HU value (right vertical axis) on line profiles (a)-(c) across vessels of different sizes, and (d) across two nearby vessels. The horizontal axis lists the point numbers on the line profiles. Jacobian values are estimated from SICLE resulting transformation, and from LITS resulting transformations using the B-Spline lattice grid size of 4 mm, 8 mm and 16 mm.

acceptable accuracy and time cost. In comparison, the Jacobian from SICLE is too smooth to be used to detect the deformation of small local features.

The Jacobian of the transformation can be used to measure local volume deformation. Fig. 3 shows that vessels have much smaller volume changes comparing with parenchyma tissue and airways during breathing cycle. In addition, since the CT images were acquired with subjects in the supine orientation, an obvious dorsal to ventral gradient is noticed on Fig. 3 and Fig. 4. This is consistent with the well known physiology that subjects positioned in the supine posture have more ventilation in the dorsal region than in the ventral region.

5 Conclusion

We described the LITS image registration method that utilizes both intensity and landmark information to register 3D CT images of lung at different pressures. Forward and reverse transformations between two images were jointly

estimated to minimize the inverse consistency error. Landmarks were selected at major vascular tree bifurcations. They were used partly for registration and partly for validation. A recently proposed intensity similarity metric SSTVD [7] was used to ensure the parenchyma tissue volume preserves during breathing cycle. The registration accuracy of LITS evaluated through measurements of landmark error, fissure positioning error, and relative overlap were better than that of SICLE which proves that this landmark-and-intensity driven method can match two lung images with large deformations effectively.

In the future, we plan to combine landmark, contour, surface and intensity based image registrations to minimize registration artifacts that negatively impact analysis. Contours such as the centerline of airways and vessels can be registered by matching landmarks defined at equally spaced intervals along the contour. Our hypothesis is that a method that uses all the correspondence information regarding the lung image registration task will produce a better result than any single type of information [15].

6 Acknowledgments

The authors would like to thank Youbing Yin for his assistance of understanding and implementing the tissue volume preserving measure. This work was supported in part by the NIH grants HL079406, HL64368, HL080285, CA129022, and EB004126.

References

1. Reinhardt, J.M., Ding, K., Cao, K., Christensen, G.E., Hoffman, E.A., Bodas, S.V.: Registration-based estimates of local lung tissue expansion compared to xenon-CT measures of specific ventilation. *Medical Image Analysis* **12**(6) (2008) 752–763 DOI: 10.1016 / j.media.2008.03.007.
2. Guerrero, T., Sanders, K., Noyola-Martinez, J., Castillo, E., Zhang, Y., Tapia, R., Guerra, R., Borghero, Y., Komaki, R.: Quantification of regional ventilation from treatment planning CT. *Int. J. Radiation Oncology Biol. Phys.* **62**(3) (2005) 630–634
3. Guerrero, T., Sanders, K., Castillo, E., Zhang, Y., Bidaut, L., Komaki, T.P.R.: Dynamic ventilation imaging from four-dimensional computed tomography. *Phys Med Biol.* **51**(4) (2006) 777–791
4. Christensen, G.E., Song, J.H., Lu, W., Naqa, I.E., Low, D.A.: Tracking lung tissue motion and expansion/compression with inverse consistent image registration and spirometry. *Med Physics* **34**(6) (2007) 2155–2165
5. Sarrut, D., Boldea, V., Miguët, S., Ginestet, C.: Simulation of four-dimensional ct images from deformable registration between inhale and exhale breath-hold CT scans. *Medical Physics* **33**(3) (2006) 605–617
6. Gorbunova, V., Lo, P., Ashraf, H., Dirksen, A., Nielsen, M., de Bruijne, M.: Weight preserving image registration for monitoring disease progression in lung CT. In: MICCAI 2008. Volume LNCS 5242., Springer (2008) 863–870
7. Yin, Y., Hoffman, E.A., Lin, C.L.: Mass preserving non-rigid registration of CT lung images using cubic B-spline. *Medical Physics* **36**(9) (2009) In press.

8. Hu, S., Hoffman, E.A., Reinhardt, J.M.: Automatic lung segmentation for accurate quantitation of volumetric X-ray CT images. *IEEE Trans. on Medical Imaging* **20** (2001) 490–498
9. Ukil, S., Reinhardt, J.M.: Anatomy-guided lung lobar surface detection in X-ray CT images. *IEEE Trans. Medical Imaging* **28**(2) (2009) 202–214
10. Murphy, K., van Ginneken, B., Pluim, J., Klein, S., Staring, M.: Semi-automatic reference standard construction for quantitative evaluation of lung CT registration. In: *Proc. of International Conference on Medical Image Computing and Computer-Assisted Intervention 2008*. Volume 5242. (2008) 1006–1013
11. Christensen, G., Johnson, H.: Consistent image registration. *IEEE Trans. Med. Imaging* **20**(7) (2001) 568–582
12. Kybic, J.: *Elastic Image Registration Using Parametric Deformation Models*. PhD thesis, Swiss Federal Institute of Technology Lausanne, EPFL, Lausanne, Switzerland (2001)
13. Kybic, J., Unser, M.: Fast parametric elastic image registration. *IEEE Transactions on Image Processing* **12**(11) (2003) 1427–1442
14. Byrd, R.H., Lu, P., Nocedal, J., Zhu, C.: A limited memory algorithm for bound constrained optimization. *SIAM J. Sci. Comput.* **16**(5) (1995) 1190–1208
15. Miller, M., Banerjee, A., Christensen, G., Joshi, S., Khaneja, N., Grenander, U., Matejic, L.: Statistical methods in computational anatomy. *Statistical Methods in Medical Research* **6** (1997) 267–299